Applied Surface Science 294 (2014) 49–57

Contents lists available at ScienceDirect

Applied Surface Science

journal homepage: www.elsevier.com/locate/apsusc

Droplets engulfing on a filament

Xiang-Fa Wu*, Meng Yu, Zhengping Zhou, Amol Bedarkar, Youhao Zhao

Department of Mechanical Engineering, North Dakota State University, Fargo, ND 58108-6050, USA

ARTICLE INFO

Article history:
Received 16 September 2013
Received in revised form
17 December 2013
Accepted 17 December 2013
Available online 2 January 2014

Keywords:
Wetting and engulfing
Droplets
Surface morphology
Young–Laplace equation
Surface science

ABSTRACT

Two immiscible droplets wetting on a filament may assume engulfing, partial-engulfing, or non-engulfing morphology that depends on the wetting behavior and geometries of the resulting droplet-on-filament system. This paper studies the wetting behavior of two immiscible droplets contacting and sitting symmetrically on a straight filament. A set of ordinary differential equations (ODEs) is formulated for determining the wetting morphology of the droplet-on-filament system. In the limiting case of engulfing or non-engulfing, the morphology of the droplet-on-filament system is determined in explicit form. In the case of partial-engulfing, surface finite element method is further employed for determining the wetting morphology, surface energy, and internal pressures of droplets of the system. Numerical scaling study is performed to explore their dependencies upon the wetting properties and geometries of the system. The study can be applicable for analysis and design of textiles with tailorable wetting properties and development of novel multifunctional fibrous materials for environmental protection such as oil-spill sorption, etc.

1. Introduction

The phenomena of wetting and wicking of liquids on surface are ubiquitous and commonly observed in nature, everyday life and engineering practices. We may recall the shinning morning dews sitting on a grass thread or a spider web and wonder how they formed and where they would go; we may also wonder the water repellency of bird feathers and the superhydrophobic nature of lotus leaves. Historically, nature provides extensive examples and raw models for humans to study, explore, innovate, and exploit these fascinating phenomena for various engineering applications. As a matter of fact, wetting and wicking of liquids on surface has been a vibrant topic of science and engineering with increasing investigations in the past decades [1–10]. Due to the importance and ubiquities of droplet-on-filament systems, their wetting behavior has been under intensive research for a long time. For instance, chemists and engineers in textile industry are interested in designable and tailorable dyeing, cleaning and waterproof properties of natural and synthetic fabrics via surface engineering including adoption of proper surfactants and surface treatment, etc. Recently scientists and engineers are also eager to understand the wetting behavior of oil/water mixture on plant leaves, bird feathers and other fibrous materials for the purpose of environmental protection such as oil-spill sorption and environmental remedy in the aftermath of the BP oil leakage in the Gulf of Mexico.

To date, substantial progress has been made to understanding the wetting and wicking phenomena of droplet-on-filament systems. In the simplest case of a droplet wetting axisymmetrically on a filament as shown in Fig. 1(a), Carroll first obtained the explicit solution to the barrel-shaped droplet morphology [11]. Several follow-up refinements have been made to further consider the droplet roll-up and spreading behavior and enhance the accuracy in extracting the contact angle from wetting experiments based on various droplet-on-filament systems [12–15]. In addition, by extending Carroll's work [11], Wu et al. [16] and Liu et al. [17] considered the effect of fiber deformation on the wetting behavior of a droplet wetting on a soft micro/nanofiber. Du et al. examined the profile of a droplet at the tip of a filament [18]. Brochard [19] and Neimark [20] formulated the kinetic and thermodynamic theories on the stability and spreading behavior of liquid droplets and films on filaments involving the disjoining pressure. Besides, Chen et al. [21] considered the wicking kinetics of a droplet wetting on a microfiber yarn. Lorenceau and Quéré [22] investigated the spreading of droplets on a tapered filament and concluded that the droplets move toward the region of lower curvature and the driving force is the gradient of Laplace pressure; Lorenceau et al. [23] also studied the capture of droplets impacting on a horizontal fiber and a kinetic relation was gained. When taking into account the effect of gravity, Huang et al. [24], Gilet et al. [25,26], and Duprat et al. [27] identified the conditions for the stability and sliding of droplets on inclined and vertically-positioned fibers, which were validated by their experiments. Furthermore, a droplet sitting on a microfiber may assume a barrel- or clamshell-shaped morphology, which depends upon the fiber diameter, droplet volume and contact

* Corresponding author. Tel.: +1 701 231 8836; fax: +1 701 231 8913.
E-mail address: Xiangfa.wu@ndsu.edu (X.-F. Wu).

0169-4332/$ – see front matter © 2014 Elsevier B.V. All rights reserved.
http://dx.doi.org/10.1016/j.apsusc.2013.12.100

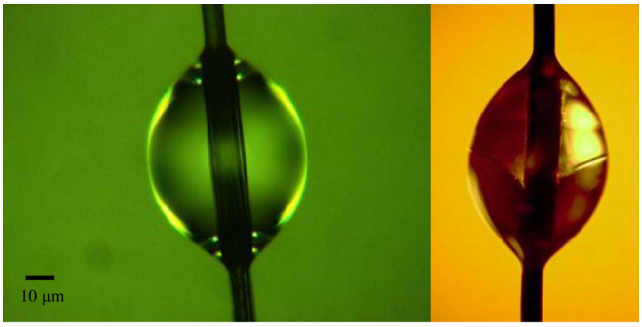

Fig. 1. Optical micrographs of (a) a barrel-shaped epoxy droplet wetting on a carbon fiber and (b) two immiscible droplets of polyacrylonitrile (PAN)-*N*,*N*-dimethylformamide (DMF)/isophorone diisocyanate (IPDI) partial-wetting on a carbon fiber (with the interface at the middle).

angle. McHale et al. [28,29] have determined the critical droplet volume for morphology transition between barrel- and clamshell-shaped droplets wetting on filaments at varying contact angle by using a surface finite element method (SFEM) [30,31]. McHale and his coworkers' predictions were well correlated to the roll-up condition by Carroll [12] and their experimental observations [28,29]. By extending McHale's works [28,29], Chou et al. further considered the effect of gravity on the morphology transition of droplet-on-filament between the barrel and clamshell shapes, and their numerical simulations indicated that the stable droplet volume is noticeably decreased by gravity [32]. Similarly, de Ruiter et al. studied the morphology transition of buoyant droplets on a filament using a well controlled electrowetting setup [33].

Beyond monolithic droplets wetting on a filament, several works have also been performed to understand the wetting and spreading behavior of a droplet sitting on multiple fibers. Among others, Princen [34–36] first considered the simplest cases of wetting and spreading of liquids in aligned multi-fiber systems, in which an asymptotic analysis was conducted for determining the capillary rises and wetting lengths in two and multiple vertically/horizontally positioned filaments. Keis et al. indicated the potential of utilizing a pair of parallel microfibers to manipulate small quantity of liquids in micro liters [37]. Their measurements showed that the wicking kinetics of a droplet spreading on such a fiber pair roughly obeyed the Lucas–Washburn law [38,39] such that given a fiber spacing, the growing wetting length of the meniscus is proportional to the complete wicking time (*i.e.*, the time interval from the start of droplet spreading to its disappearance). Yet, a droplet sitting on a pair of two parallel fibers may assume a barrel-shaped droplet, which completely enwraps the two fibers, or a liquid bridge, which only partially wets the internal surfaces and therefore partially enwraps the two fibers. Such a morphology transition could further influence the liquid spreading. Similar to the work by McHale et al. [28,29], Wu et al. [40,41] determined the characteristic wetting curves as the phase diagram boundaries between the morphologies of barrel-shaped droplet and liquid bridge spanning on two aligned filaments. Based on controlled droplet-on-fiber systems, Protiere et al. [42] recently identified such morphology transition based on an experimental morphology diagram and discovered the transition hysteresis, a wetting phenomenon commonly observed in the process of droplet spreading. In addition, Bedarkar and Wu [43] and Virozub et al. [44] determined the capillary torque induced by a droplet bridge formed between two misaligned filaments, where symmetry breaking of a droplet bridge triggers the nonsymmetric capillary force that is responsible for the capillary torque.

Moreover, the capillary force due to droplets wetting and spreading on filaments may also result in noticeable elastic deformation, *i.e.*, elastocapillary effect, which further influences the interaction between the droplets and filaments [16,45–53]. Such an elastocapillary effect could be exploited for assembly of microdevices [54–56]. The capillary force due to liquid wetting and spreading in fiber networks may also lead to fiber collapse, contact and fusion [57–60], which further affect the mechanical response of fiber networks [61].

Yet, all the above studies were focused on monolithic droplets wetting on a filament or multi-fibers. To authors' knowledge, no systematic investigations have been reported yet on dissimilar liquids wetting on filaments though such phenomena are commonly observed in nature and engineering such as cleaning of oil–water mixture on textiles and sorption and recovering of oil spills in ocean, etc. Thus, as natural extension of the prior studies, in this work we initiate the theoretical study on determining the morphology and surface energy of two immiscible droplets wetting on a filament. A set of governing ordinary different equations (ODEs) will be formulated. In parallel, a computational microfluidic model of the present problem will be established; the wetting morphology, surface energy, and internal pressure of the droplet-on-filament system are determined by SFEM: *Surface Evolver* [30,31]. Dependencies of the droplet morphology, surface energy, and internal pressure of the two immiscible droplets on a filament upon the droplet surface tension, contact angle, droplet volume, and filament diameter will be examined. In consequence, discussions on the results and potential applications of the present study will be addressed.

2. Problem formulation and solution

2.1. General governing equations of droplets wetting on filaments

Consider two immiscible droplets partial-engulfing axisymmetrically on a filament of uniform circular cross-section as shown in Fig. 1(b). Fig. 2 is the corresponding schematic diagram with a proper coordinate system. For the convenience of derivation hereafter, except for those designated specifically, parameters and variables with subscripts "1", "2", and "12" are attached to droplet 1, droplet 2, and the interface between droplets 1 and 2, respectively, while symbols without subscripts are applicable to either droplet. Due to the axisymmetry of the droplet-on-filament system, the principal radii R_1 and R_2 of curvature of each droplet surface of the droplets at locus $[x, y(x)]$ can be expressed:

$$\frac{1}{R_1} = \frac{1}{(y\mathrm{cosec}\,\psi)} = \frac{1}{[y(x)\sqrt{1+[y'(x)]^2}]}, \tag{1}$$

$$\frac{1}{R_2} = \frac{-y''(x)}{\sqrt{\{1+[y'(x)]^2\}^3}}. \tag{2}$$

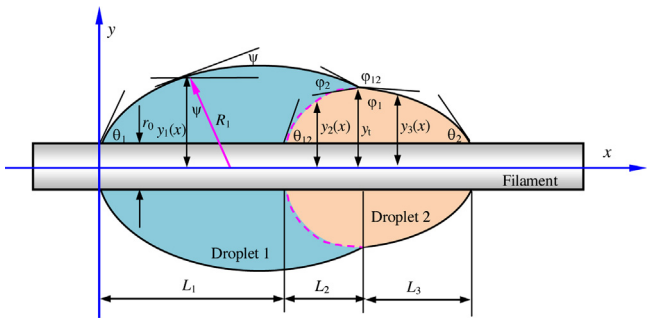

Fig. 2. Geometries of two immiscible droplets partial-engulfing axisymmetrically on a filament.

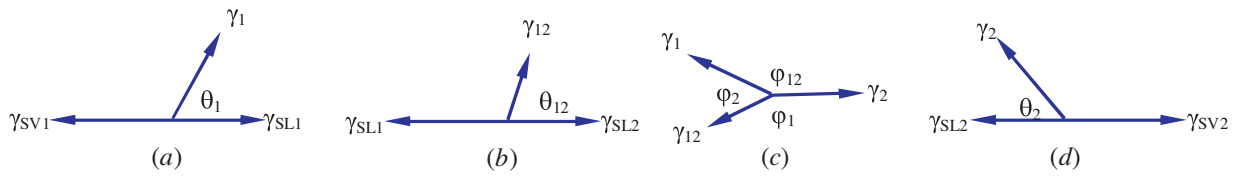

Fig. 3. Schematic diagrams of three-phase intersection. (a) Left droplet/fiber/gas intersection; (b) internal droplet/droplet/fiber intersection; (c) droplet/droplet/gas intersection at surface; (d) right droplet/fiber/gas interaction.

Thus, Young–Laplace formula specifies the surface morphology of the liquid droplets [9,10,15], which reads

$$\gamma\left(\frac{1}{R_1}+\frac{1}{R_2}\right)=\Delta p, \tag{3}$$

where Δp is the droplet pressure defined as

$$\Delta p = p_L - p_V. \tag{4}$$

In the above, p_L and p_V are the pressures inside and outside the droplet, respectively. As a result, the governing ODE for each curvilinear segment of the droplet profile can be obtained by substituting (1) and (2) into (3) as

$$\gamma\left\{\frac{1}{\{y(x)\sqrt{1+[y'(x)]^2}\}}-\frac{y''(x)}{\sqrt{\{1+[y'(x)]^2\}^3}}\right\}=\Delta p. \tag{5}$$

Eq. (5) has the first integration:

$$\frac{1}{\sqrt{1+[y'(x)]^2}}=Ay(x)+\frac{B}{y(x)}, \tag{6}$$

where

$$A=\frac{\Delta p}{(2\gamma)}, \tag{7}$$

and B is an integration constant to be determined according to the contact angle at the droplet end.

In addition, there are three boundary conditions (BCs) of contact angle at the right, internal and left ends of the droplets and one three-phase intersection condition at the outer surface, which are specified as shown in Fig. 3. The three-phase intersection of droplet/droplet/gas as shown in Fig. 3(c) gives [61]

$$\frac{\sin\varphi_1}{\gamma_1}=\frac{\sin\varphi_2}{\gamma_2}=\frac{\sin\varphi_{12}}{\gamma_{12}}. \tag{8}$$

There exist two trivial limiting cases of engulfing and non-engulfing, in which the morphology and surface energy of the droplet-on-filament systems can be determined explicitly based on the solution of a monolithic droplet wetting on a filament [15]. In the general case of partial-engulfing, to avoid the complicated discussions of various connecting conditions in solving Eq. (6), we will establish a computational microfluidic droplet model and employ an efficient SFEM to determine the morphology and surface energy of the droplet-on-filament systems and their dependencies upon the model parameters.

2.2. Engulfing and non-engulfing of two immiscible droplets on a filament

In the case of two immiscible droplets engulfing on a filament, one droplet is completely enwrapped within the second one as illustrated in Fig. 4. This situation happens when the interfacial energy between two droplets is lower than the surface tension of either droplet since engulfing can reduce the total potential energy of the droplet-on-filament system. In this case, the morphologies of

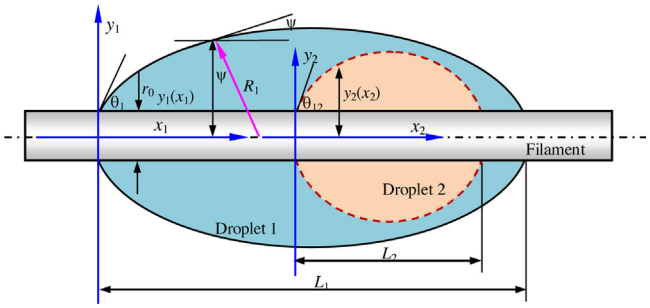

Fig. 4. Schematic diagram of two immiscible droplets engulfing on a filament.

the two droplets can be determined by solving Eq. (6) for a monolithic barrel-shaped droplet wetting on a filament (left-half droplet due to the symmetry) [11,15] such that

$$x_i=\int_{y_i}^{y_{i0}}\frac{(y_i^2+\lambda_i r_0 y_{i0})}{\sqrt{(y_{i0}^2-y_i^2)(y_i^2-\lambda_i^2 r_0^2)}}dy_i,\ (i=1,2) \tag{9}$$

where $i=1$ and 2 are corresponding to the first and second droplets, respectively,

$$\lambda_1=\frac{(y_{10}\cos\theta_1-r_0)}{(y_{10}-r_0\cos\theta_1)}, \tag{10}$$

$$\lambda_2=\frac{(y_{20}\cos\theta_{12}-r_0)}{(y_{20}-r_0\cos\ \theta_{12})}, \tag{11}$$

x_i ($i=1, 2$) are defined with the origin located at the left end of droplets 1 and 2, respectively, y_{i0} ($i=1, 2$) are the peak radii (at the middle) of droplets 1 and 2 along the vertical symmetric axis, respectively.

Thus, the wetting lengths L_i ($i=1, 2$) of droplets 1 and 2 on the filament can be determined by setting $y_i=r_0$ ($i=1, 2$) as

$$L_i=\int_{r_0}^{y_{i0}}\frac{(y_i^2+\lambda_i r_0 y_{i0})}{\sqrt{(y_{i0}^2-y_i^2)(y_i^2-\lambda_i^2 r_0^2)}}dy_i\quad(i=1,2) \tag{12}$$

In the above, y_{i0} ($i=1, 2$) can be determined according to the volumes of the two droplets:

$$V_1+V_2=\int_{r_0}^{y_{10}}\frac{y_1^2(y_1^2+\lambda_1 r_0 y_{10})}{\sqrt{(y_{10}^2-y_1^2)(y_1^2-\lambda_1^2 r_0^2)}}dy_1, \tag{13}$$

$$V_2=\int_{r_0}^{y_{20}}\frac{y_2^2(y_2^2+\lambda_2 r_0 y_{20})}{\sqrt{(y_{20}^2-y_2^2)(y_2^2-\lambda_2^2 r_0^2)}}dy_2. \tag{14}$$

Each of the above integral equations can be conveniently solved by means of numerical methods developed in our previous studies [15]. Consequently, plugging y_{i0} ($i=1, 2$) into (9) and (12) determines the morphologies and wetting lengths of the two droplets, respectively.

In the case of two droplets wetting but non-engulfing on a filament, the wetting behaviors of the two droplets are independent. The solutions to the morphology, wetting length, and surface

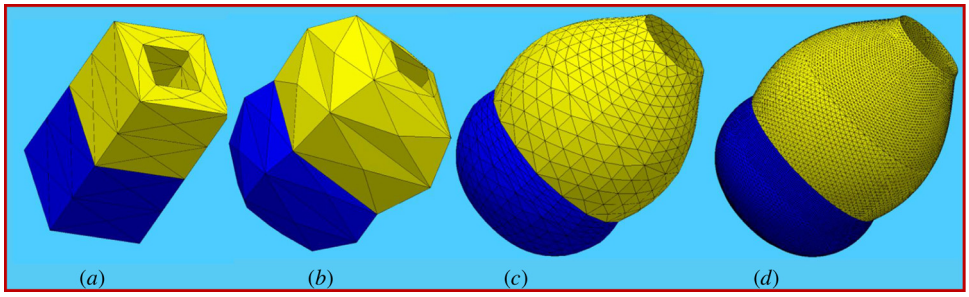

Fig. 5. Surface finite element analysis of two immiscible droplets partial-wetting on a filament by *Surface Evolver*. (a): Two super volume elements to represent two immiscible droplets on the filament. (b): Droplet morphology after two numerical iterations. (c): Well stable droplet morphology formed after a few numerical iterations and mesh refinements. (d): Wetting droplet morphology close to the final state after multiple numerical iterations and mesh refinements [The final droplet morphology was obtained using much finer mesh while it is very close to the morphology shown in (d)]. Geometrical parameters: droplet volumes: $V_1 = 128$ (yellow droplet), $V_2 = 80$ (blue droplet); fiber radius $r = 1.5$; wetting parameters: contact angles: $\theta_1 = 35^\circ$ (yellow); $\theta_2 = 80^\circ$ (blue); surface tensions: $\gamma_1 = 0.5$ (yellow); $\gamma_2 = 1.0$ (blue); interfacial tension between two droplets: $\gamma_{12} = 0.7$.(For interpretation of the references to color in this figure legend, the reader is referred to the web version of the article.)

energy of each droplet are the same as those for a monolithic droplet wetting on a filament [15].

2.3. Partial-engulfing of two immiscible droplets wetting on a filament

In this case, it is inconvenient to directly solve Eq. (6) at three droplet portions as shown in Fig. 2 under three droplet-end BCs and one three-phase interaction condition at the outer droplet surface (Fig. 3) due to involvement of multi-valued functions. Thus, a partial-engulfing droplet model is established and the efficient SFEM *Surface Evolver* [30,31] is employed for directly determining the morphology, surface energy and capillary pressure of two partial-engulfing droplets on a filament. Based on the minimum potential energy of droplet-on-filament system, SFEM is capable of searching for the morphology of equilibrium state of the two

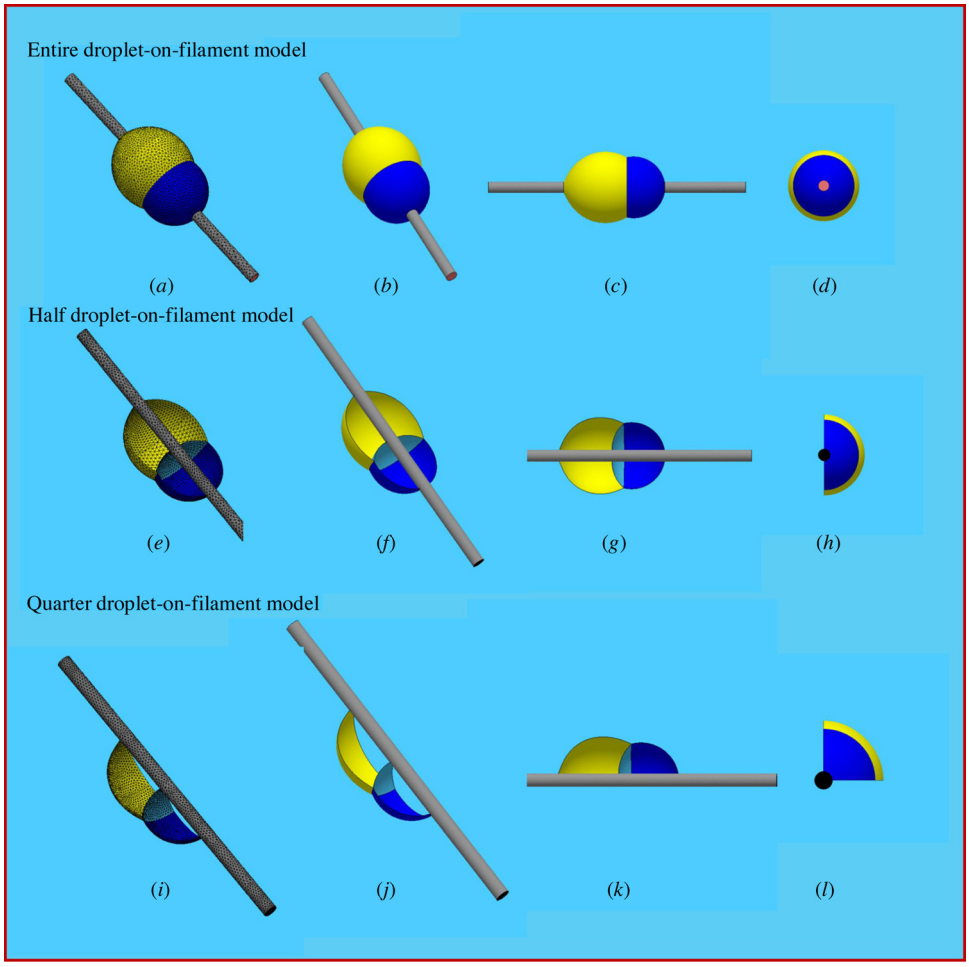

Fig. 6. Comparison of droplet wetting morphologies based on entire-, half-, and quarter-droplet models of two immiscible droplets partial-engulfing on a fiber by *Surface Evolver*. Column 1: SFEM mesh at the final state; Column 2: 3D view; Column 3: front view; Column 4: top view. Geometrical parameters: droplet volumes: $V_1 = 128$ (yellow droplet), $V_2 = 80$ (blue droplet); fiber radius $r = 1.5$; Wetting parameters: contact angles: $\theta_1 = 35^\circ$ (yellow); $\theta_2 = 80^\circ$ (blue); surface tensions: $\gamma_1 = 0.5$ (yellow); $\gamma_2 = 1.0$ (blue); interfacial tension between two droplets: $\gamma_{12} = 0.7$.(For interpretation of the references to color in this figure legend, the reader is referred to the web version of the article.)

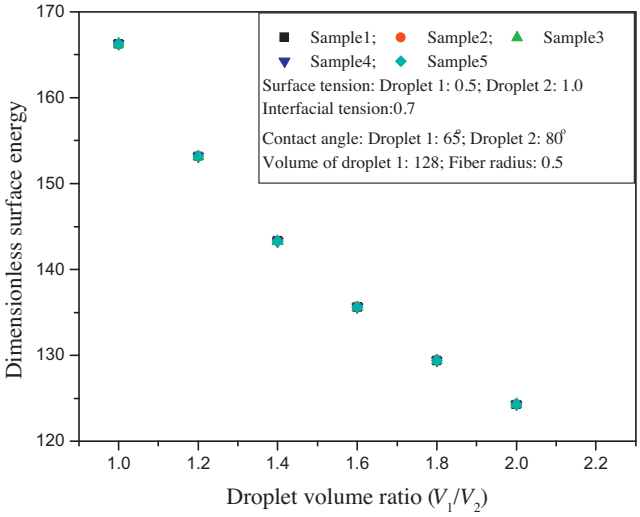

Fig. 7. Variation of the global surface energy of two partial-engulfing droplets on a fiber with respect to the droplet volume ratio.

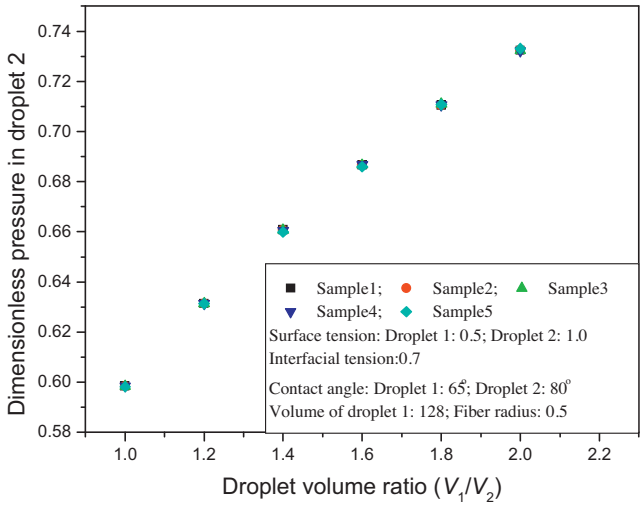

Fig. 9. Variation of the pressure of droplet 2 of two partial-engulfing droplets on a fiber with respect to the droplet volume ratio.

partial-engulfing droplets on a filament via minimizing the global surface energy of system:

$$\Pi = \min\{\sum_{i=1}^{2}[\gamma_i A_{L_iV} + (\gamma_{SL_i} - \gamma_{SV})A_{SL_i}] + \gamma_{12}A_{L_1L_2}\}, \quad (15)$$

under given geometrical constraints (*i.e.*, the constant droplet volumes and geometrical constraints of filament surfaces). In the above, γ_{SL_i} and γ_{SV} are respectively the interfacial tensions of solid–liquid and solid–vapor, A_{L_iV} and A_{SL_i} are respectively the liquid–vapor and solid–liquid interfacial areas, and $A_{L_1L_2}$ are the interfacial area between two partial-engulfing droplets. In this study, the computational procedure of (15) is implemented by using a public domain SFEM package: *Surface Evolver* by Brakke [30,31]. It has been demonstrated that *Surface Evolver* is an efficient, universal simulation tool capable of solving a wealth of wetting problems involving complex surface facets and multiple liquids.

During the numerical simulation based on *Surface Evolver*, the SFEM model of two partial-engulfing droplets on a filament is built up by first defining two super volume elements that represent the two partial-engulfing droplets as shown in Fig. 5(a). Two groups of model parameters are defined as requested by *Surface Evolver*, *i.e.*, geometric parameters: volumes (*i.e.*, V_1 and V_2) of two droplets and filament radius (r), wetting parameters: two contact angles (*i.e.*, θ_1 and θ_2) between the droplets and filament, surface tensions (*i.e.*, γ_1 and γ_2) of two droplets, and interfacial tension (γ_{12}) between two droplets. Similar to those adopted by Wu et al. [40,41] and others, the global surface energy of the droplet-on-filament system is used as the criterion to search for the critical droplet morphology at given geometrical and wetting parameters. Since the numerical solving process of *Surface Evolver* is based on numerical iteration with slow convergence rate at the situation of very fine mesh and very large number of nodes. Therefore, special cares have been taken in the course of generating input data file and refining the droplet mesh in order to accelerate the numerical convergence and maintain the numerical stability. The numerical iteration is terminated when the relative numerical error of the global surface energy of the system is below 1%. Fig. 5 shows the typical snapshots during a numerical process (the filament is not plotted). It can be observed that the wetting morphology of the droplet-on-filament system secures very good stability after only a few iterations and then maintain such stable morphology till the end of the numerical process. In addition, due to the axisymmetry of the droplet-on-filament system, half- and quarter-droplet models are further built up and

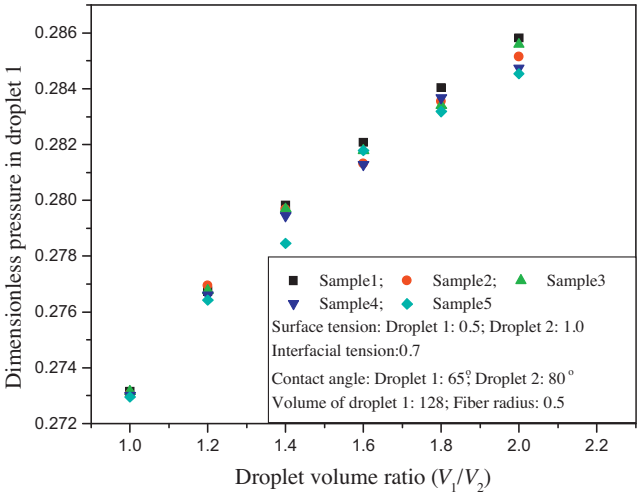

Fig. 8. Variation of the pressure of droplet 1 of two partial-engulfing droplets on a fiber with respect to the droplet volume ratio.

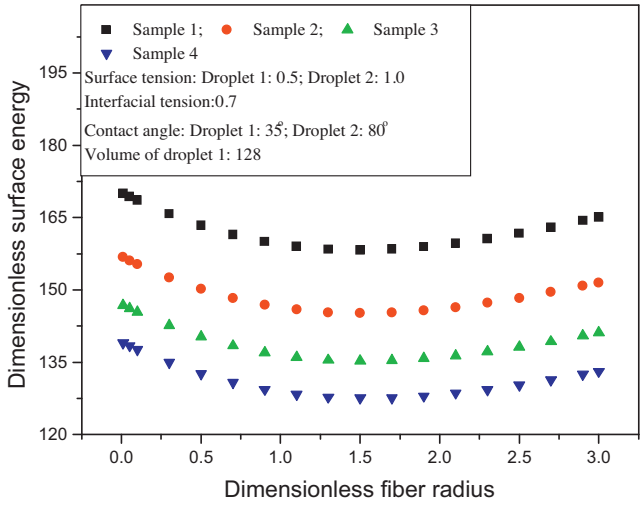

Fig. 10. Variation of the global surface energy of two partial-engulfing droplets on a filament with respect to the fiber radius.

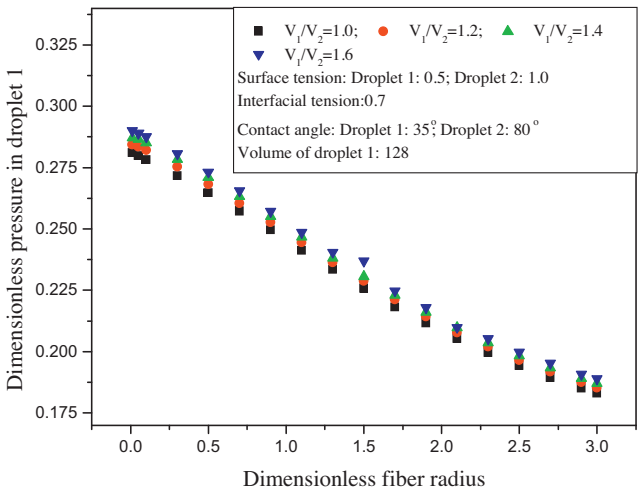

Fig. 11. Variation of the pressure of droplet 1 of two partial-engulfing droplets on a filament with respect to the fiber radius.

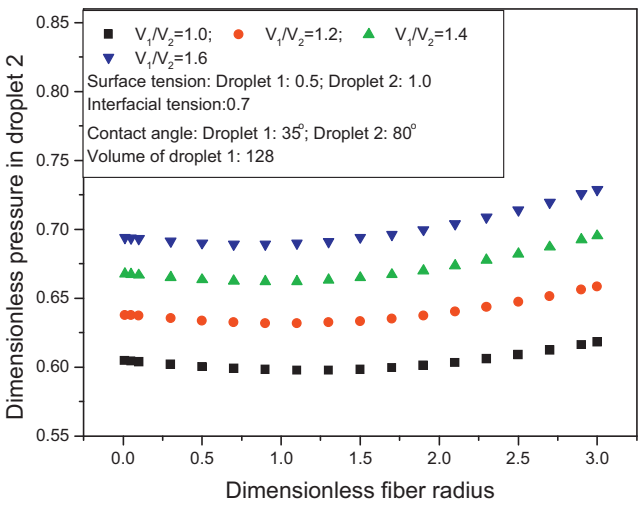

Fig. 12. Variation of the pressure of droplet 2 of two partial-engulfing droplets on a filament with respect to the fiber radius.

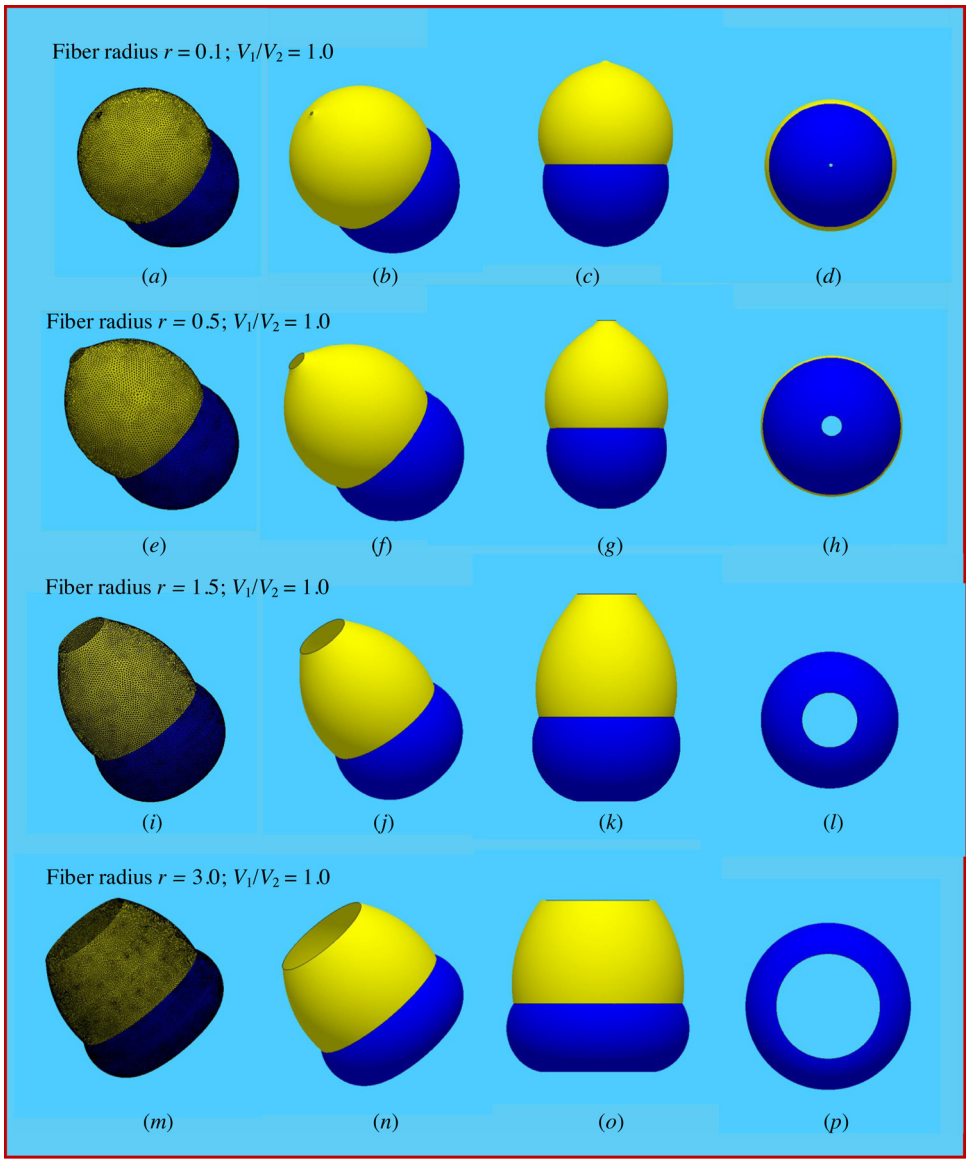

Fig. 13. Wetting morphologies of two partial-engulfing droplets on a filament with varying fiber radius. Column 1: SFEM mesh at the final state; Column 2: 3D view; Column 3: front view; Column 4: top view. Geometrical parameters: volume of droplet 1: $V_1 = 128$; wetting parameters: contact angles: $\theta_1 = 35^\circ$ and $\theta_2 = 80^\circ$; surface tensions: $\gamma_1 = 0.5$ and $\gamma_2 = 1.0$; interfacial tension between two droplets: $\gamma_{12} = 0.7$.

simulated to validate the entire-droplet model (Fig. 5). Numerical results indicate that these droplet models are capable of predicting highly accurate surface energy and droplet internal pressures. Fig. 6 compares a few wetting morphologies of the entire-, half-, and quarter-droplet models with the same geometrical and wetting parameters. It can be observed that the wetting morphologies of the droplets based on the three droplet models are the same, which also validate the present droplet models.

2.4. Numerical scaling analysis of two partial-engulfing immiscible droplets on a filament

The above droplet-on-filament models are further exploited for examining dependencies of the surface energy and droplet internal pressure of two partial-engulfing droplets on a filament upon the droplet volume ratio and fiber radius. It needs to be mentioned that all the physical parameters used in the present simulations are dimensionless, which means that when assigning proper units to a few parameters, the units of the rest parameters are specified properly. For instance, if assigning "N/mm" and "mm" as the units of surface/interfacial tension and fiber radius, respectively, then the unit of surface energy would be "N mm" and the unit of droplet volume would be "mm^3". Other unit conversions even with scaling can be derived correspondingly. In the following, two groups of numerical simulations are performed for scaling analysis. The selection of specific model parameters does not limit the universal nature of the present droplet models in solving broad wetting problems of droplet-on-filaments. In the first set of simulations, the following model parameters are fixed: geometrical parameter $V_1 = 128$ and fiber radius $r = 0.5$; wetting parameters: contact angles: $\theta_1 = 65^\circ$ and $\theta_2 = 80^\circ$; surface tensions: $\gamma_1 = 0.5$ and $\gamma_2 = 1.0$; interfacial tension between two droplets: $\gamma_{12} = 0.7$, while the volume of droplet 2 decreases with the droplet volume ratio V_1/V_2 from 1.0 to 2.0 such that six discrete V_1/V_2 ratios are sampled ($V_1/V_2 = 1.0$, 1.2, 1.4, 1.6, 1.8, and 2.0). At each sampled V_1/V_2 ratio, five simulations are executed to ensure the repetitiveness of the droplet model; half- and quarter-droplet models are also utilized to validate the robustness of the entire-droplet model. Figs. 7–9 show the variations of the surface energy and droplet internal pressures with respect to the varying droplet volume ratio (V_1/V_2). It can be observed from Figs. 7–9 that the numerical experiments show very good numerical convergences, corresponding to the robust droplet

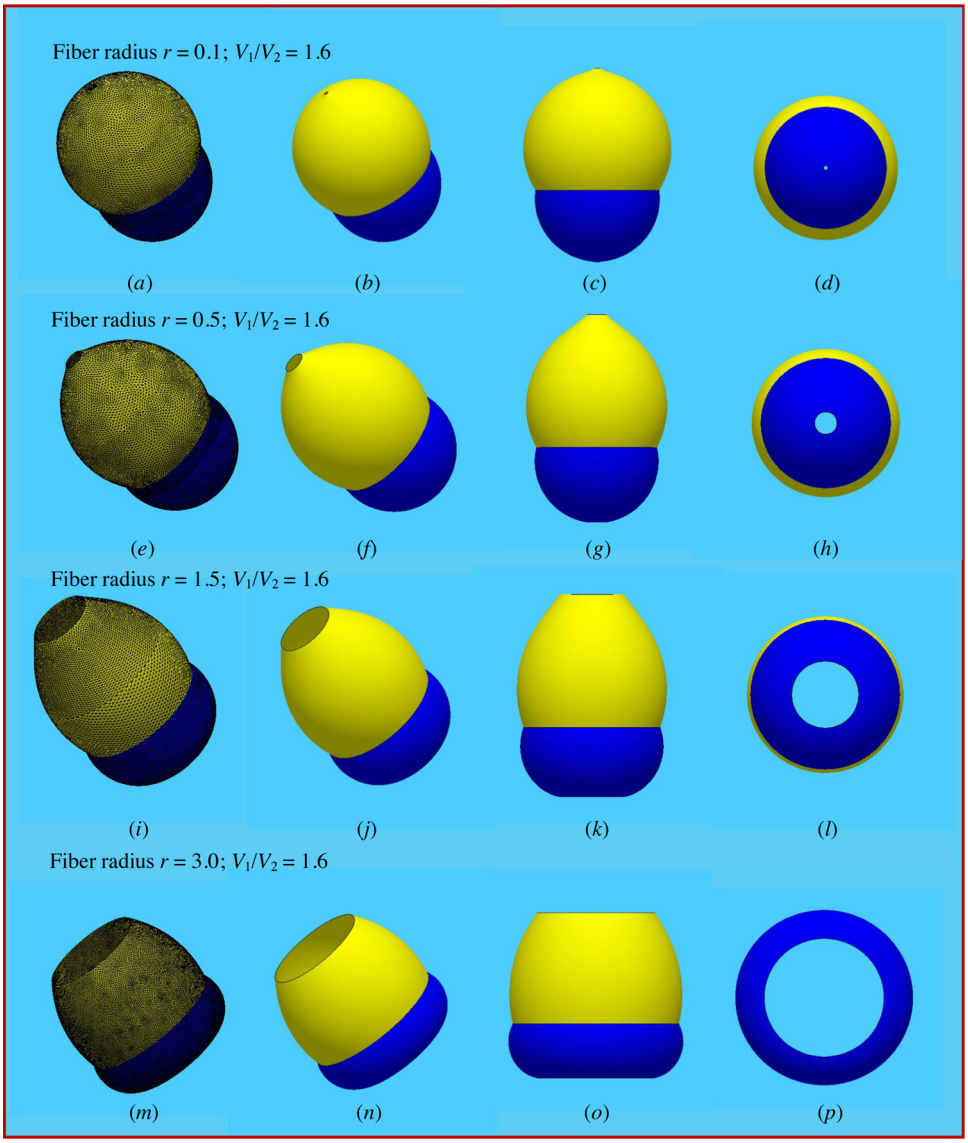

Fig. 14. Wetting morphologies of two partial-engulfing droplets on a fiber with varying diameter. Column 1: SFEM mesh at the final state; Column 2: 3D view; Column 3: front view; Column 4: top view. Geometrical parameters: volume of droplet 1: $V_1 = 128$; wetting parameters: contact angles: $\theta_1 = 35^\circ$ and $\theta_2 = 80^\circ$; surface tensions: $\gamma_1 = 0.5$ and $\gamma_2 = 1.0$; interfacial tension between two droplets: $\gamma_{12} = 0.7$.

model aforementioned and showed in Figs. 5 and 6. Fig. 7 indicates that at the given model parameters, the global surface energy of two partial-engulfing droplets on a filament decreases nearly linearly with increasing droplet volume ratio. This observation can be understood that given the volume of droplet 1 (V_1), the volume of droplet 2 (V_2) decreases with increasing droplet volume ratio (V_1/V_2), which leads to the decrease of the total volume and surface area of the droplet-on-filament system, *i.e.*, decreasing global surface energy. Figs. 8 and 9 show that the internal pressure in both droplets increases nearly linearly with increasing droplet volume ratio. Herein, with increasing droplet volume ratio, the volume of droplet 2 (V_2) decreases, corresponding to the decrease of mean principal radius of curvature of droplet 2, *i.e.*, the increase of internal pressure of droplet 2 according to Young–Laplace formula (3). In addition, the increased pressure in droplet 2 further deforms droplet 1, resulting in the decrease of the mean principal radius of curvature of droplet 1, *i.e.*, the increase of internal pressure of droplet 1 as shown in Fig. 8.

In the second group of simulations, the following model parameters are specified: geometrical parameter $V_1 = 128$; wetting parameters: contact angles: $\theta_1 = 35^\circ$ and $\theta_2 = 80^\circ$; surface tensions: $\gamma_1 = 0.5$ and $\gamma_2 = 1.0$; interfacial tension between two droplets: $\gamma_{12} = 0.7$. Four droplet volume ratios are used ($V_1/V_2 = 1.0$, 1.2, 1.4, and 1.6), and the fiber radius r varies from 0.01 to 3.0. Figs. 10–12 show the variations of the surface energy and droplet internal pressures with respect to the varying fiber radius. Fig. 10 indicates that given the model parameters, the global surface energy decreases with increasing droplet volume ratio (V_1/V_2) within the range of fiber radius under investigation as expected from the above simulations. In contrast, the global surface energy decreases slightly and then increases with increasing fiber radius for each droplet volume ratio specified in this study. The latter indicates that a minima of global surface energy exists at a critical fiber radius for each droplet volume ratio (V_1/V_2). In addition, Fig. 11 shows that given a droplet volume ratio (V_1/V_2), the internal pressure of the droplet 1 decreases nearly linearly with increasing fiber radius; while given a fiber radius, it also increases slightly with increasing droplet volume ratio (V_1/V_2) as predicted in the first set of simulations. Fig. 12 shows that given a droplet volume ratio (V_1/V_2), the internal pressure of droplet 2 decreases slightly and then increases continuously with increasing fiber radius, which also means that a minima of internal pressure of droplet 2 exists at a critical fiber radius. Furthermore, given a fiber radius, the internal pressure of droplet 2 increases with decreasing the droplet volume ratio (V_1/V_2), similar to those predicted in the first group of simulations.

Furthermore, variations of the droplet morphology with respect to the fiber radius at two droplet volume ratios ($V_1/V_2 = 1.0$ and 1.6) are shown in Figs. 13 and 14. It can be observed that given a fiber radius, the droplet morphology deforms with increasing droplet volume ratio (V_1/V_2). Meanwhile, given a droplet volume ratio (V_1/V_2), the droplet gradually transfers into a thinning torus on the fiber with increasing fiber radius, resulting in a lower principal radius of morphology curvature in the axisymmetric plane, *i.e.*, higher internal pressure of droplet 2.

3. Concluding remarks

The engulfing behavior of two immiscible droplets on a filament has been studied in this work. Analytic solutions to two limiting cases of droplet engulfing and non-engulfing have been determined by extending the previous studies on a barrel-shaped monolithic droplet wetting on a filament. In the case of two immiscible droplets partial-engulfing on a filament, a robust computational droplet model has been established and validated successfully. Detailed numerical simulations have been conducted using an efficient SFEM (*Surface Evolver*) for systematically examining the dependencies of model parameters on the wetting morphology, surface energy, and internal pressure of droplets of the droplet-on-filament systems. It needs to be acknowledged that the present study is still at the beginning of this research field, and quite a few outstanding issues need to be explored such as the phase diagram of describing the morphology transition among engulfing, non-engulfing, and partial-engulfing of two immiscible droplets on a filament. Yet, due to the involvement of multiple droplets, surfaces and interfaces, explicit solution to such a phase diagram might be extremely difficult to gain; purely numerical simulations based on *Surface Evolver* would also be rather challenging since *Surface Evolver* (based on traditional surface meshing) is unable to predict the topological transition (morphological transition of engulfing) of the droplet-on-filament. Thus, new efficient, suitable numerical methods are still desired for resolving such issue.

In addition, the present computational modeling also provides rich information on two immiscible droplets partial-engulfing on a filament. The numerical scaling analysis has explored the dependencies of wetting morphology, surface energy, and internal pressure of droplets of the droplet-on-filament system upon the wetting properties and geometries of the system. The present study offers a practicable tool that can be utilized for analysis and design of tailorable wetting properties of textiles and development of novel multifunctional fibrous materials for environmental protection such as oil-spill sorption, oil–water separation, targeted cleaning and liquid sorption, etc.

Acknowledgments

Partial support of the research by the National Science Foundation (NSF CMMI: 1234297), NDSU Development Foundation (FAR0021589), North Dakota Soybean Council, and NDSU New Faculty Research Initiative Grant is gratefully appreciated.

References

[1] P.G. de Gennes, Rev. Modern Phys. 57 (1985) 827.
[2] H. Gau, S. Herminghaus, P. Lenz, R. Lipowsky, Science 283 (1999) 46.
[3] R. Seemann, M. Brinkmann, E.J. Kramer, F.F. Lang, R. Lipowsky, Proc. Natl. Acad. Sci. 102 (2005) 1842.
[4] M. Alava, M. Dube, M. Rost, Adv. Phys. 53 (2004) 83.
[5] D. Bonn, J. Eggers, J. Indekeu, J. Meunier, E. Rolley, Rev. Modern Phys. 81 (2009) 739.
[6] D. Quéré, Ann. Rev. Mater. Res. 38 (2008) 71.
[7] B. Bhushan, Y.C. Jung, Prog. Mater. Sci. 56 (2011) 1.
[8] L.J. Xue, Y.C. Han, Prog. Polym. Sci. 36 (2011) 269.
[9] P.G. de Gennes, F. Brochard-Wyart, D. Quéré, Capillarity and Wetting Phenomena—Drops, Bubbles, Pearls, Waves, Springer, New York, NY, 2004 (translated by A. Reisinger).
[10] V.M. Starov, M.G. Velarde, C.J. Radke, Wetting and Spreading Dynamics, CRC, Press, Boca Raton, FL, 2007.
[11] B.J. Carroll, J. Colloid Interface Sci. 57 (1976) 488.
[12] B.J. Carroll, Langmuir 2 (1986) 248.
[13] H.D. Wagner, J. Appl. Phys. 67 (1990) 1352.
[14] B.H. Song, A. Bismarck, R. Tahhan, J. Springer, J. Colloid Interface Sci. 197 (1998) 68.
[15] X.F. Wu, Y.A. Dzenis, Acta Mech. 185 (2006) 215.
[16] X.F. Wu, A. Bedarkar, I.S. Akhatov, J. Appl. Phys. 108 (2010) 083518.
[17] J.L. Liu, J. Sun, Y. Mei, J. Appl. Phys. 114 (2013) 044901.
[18] J.M. Du, S. Michielsen, H.J. Lee, Langmuir 26 (2010) 16000.
[19] F. Brochard, J. Chem. Phys. 84 (1986) 4664.
[20] A.V. Neimark, J. Adhes. Sci. Tech. 13 (1999) 1137.
[21] X.M. Chen, K.G. Kornev, Y.K. Kamath, A.V. Neimark, Textile Res. J. 71 (2001) 862.
[22] É. Lorenceau, D. Quéré, J. Fluid Mech. 510 (2004) 29.
[23] É. Lorenceau, C. Clanet, D. Quéré, J. Colloid Interface Sci. 279 (2004) 192.
[24] Z.B. Huang, X.M. Liao, Y.Q. Kang, G.F. Yin, Y.D. Yao, J. Colloid Interface Sci. 330 (2009) 399.
[25] T. Gilet, D. Terwagne, N. Vandewalle, Appl. Phys. Lett. 95 (2009) 014106.
[26] T. Gilet, D. Terwagne, N. Vandewalle, Eur. Phys. J. E. 31 (2010) 253.
[27] C. Duprat, C. Ruyer-Quil, F. Giorgiutti-Dauphiné, Eur. Phys. J. Special Top. 166 (2009) 63.
[28] G. McHale, M.I. Newton, B.J. Carroll, Oil Gas Sci. Tech. 56 (2001) 47.

[29] G. McHale, M.I. Newton, Colloids Surf. A: Physicochem. Eng. Aspects 206 (2002) 79.
[30] K.A. Brakke, Exp. Math. 1 (1992) 141.
[31] K.A. Brakke, Surface Evolver, 2000 www.susqu.edu/facstaff/b/vrajjer/evolver
[32] T.H. Chou, S.J. Hong, Y.E. Liang, H.K. Tsao, Y.J. Sheng, Langmuir 27 (2011) 3685.
[33] R. de Ruiter, J. de Ruiter, H.B. Eral, C. Semprebon, M. Brinkmann, F. Mugele, Langmuir 28 (2012) 13300.
[34] H.M. Princen, J. Colloid Interface Sci. 30 (1969) 69.
[35] H.M. Princen, J. Colloid Interface Sci. 30 (1969) 359.
[36] H.M. Princen, J. Colloid Interface Sci. 34 (1970) 171.
[37] K. Keis, K.G. Kornev, A.V. Neimark, Y.K. Kamath, in: S. Guceri, Y.G. Gogotsi, V. Kuznetov (Eds.), Nanoengineered Nanofibrous Materials, Springer, 2004, p. 173.
[38] R. Lucas, Kollid. Zeitschrift 23 (1918) 15.
[39] E.W. Washburn, Phys. Rev. 17 (1921) 273.
[40] X.F. Wu, A. Bedarkar, K.A. Vaynberg, J. Colloid Interface Sci. 341 (2010) 326.
[41] A. Bedarkar, X.F. Wu, A. Vaynberg, Appl. Surf. Sci. 256 (2010) 7260.
[42] S. Protiere, C. Duprat, H.A. Stone, Soft Matter 9 (2013) 271.
[43] A. Bedarkar, X.F. Wu, J. Appl. Phys. 106 (2009) 113527.
[44] A. Virozub, N. Haimovich, S. Brandon, Langmuir 25 (2009) 12837.
[45] J. Bico, B. Roman, L. Moulin, A. Boudaoud, Nature 432 (2004) 690.
[46] A. Boudaoud, J. Bico, B. Roman, Phys. Rev. E 76 (2007) 060102.
[47] J.M. Aristoff, C. Duprat, H.A. Stone, Int. J. Non-Linear Mech. 46 (2011) 648.
[48] C. Duprat, J.M. Aristoff, H.A. Stone, J. Fluid Mech. 679 (2011) 641.
[49] C. Duprat, S. Protière, A.Y. Beebe, H.A. Stone, Nature 482 (2012) 510.
[50] S. Neukirch, B. Roman, B. de Gaudemaris, J. Bico, J. Mech. Phys. Solids 55 (2007) 1212.
[51] J. Hure, B. Audoly, J. Mech. Phys. Solids 61 (2013) 450.
[52] J.L. Liu, X.Q. Feng, Acta Mech. Sinica 28 (2012) 928.
[53] B. Roman, J. Bico, J. Phys. C 22 (2010) 493101.
[54] R.R.A. Syms, J. Microelectromech. Syst. 8 (1999) 448.
[55] R.R.A. Syms, E.M. Yeatman, V.M. Bright, G.M. Whitesides, J. Microelectromech. Syst. 12 (2003) 387.
[56] J.W. van Honschoten, J.W. Berenschot, T. Ondarcuhu, R.G.P. Sanders, J. Sundaram, M. Elwenspoek, N.R. Tas, Appl. Phys. Lett. 97 (2010) 014103.
[57] X.F. Wu, Y.A. Dzenis, Nanotechnology 18 (2007) 285702.
[58] X.F. Wu, Y.A. Dzenis, J. Phys. D: Appl. Phys. 40 (2007) 4276.
[59] X.F. Wu, Z.P. Zhou, W.M. Zhou, Appl. Phys. Lett. 100 (2012) 193115.
[60] X.F. Wu, Y.A. Dzenis, J. Appl. Phys. 98 (2005) 093501.
[61] J.B. Hudson, Surface Science: An Introduction, John Wiley & Sons, New York, 1998.